

Title

Study of mode II fracture on fibre-reinforced gypsum notched specimens

Authors

- Fernando Suárez. Departamento de Ingeniería Mecánica y Minera. Universidad de Jaén. Campus Científico-Tecnológico de Linares. Cinturón Sur 23700 – Linares (Jaén), Spain (ORCID: 0000-0002-8834-104X)
- Javier F. Aceituno. Departamento de Ingeniería Mecánica y Minera. Universidad de Jaén. Campus Científico-Tecnológico de Linares. Cinturón Sur 23700 – Linares (Jaén), Spain (ORCID: 0000-0002-5994-3973)
- Jesús Donaire-Ávila. Departamento de Ingeniería Mecánica y Minera. Universidad de Jaén. Campus Científico-Tecnológico de Linares. Cinturón Sur 23700 – Linares (Jaén), Spain (ORCID: 0000-0003-4764-1852)

Abstract

In this paper, two experimental tests used for studying shear fracture in quasibrittle materials are analysed by testing fibre-reinforced gypsum specimens. The main aim of this work is not to measure specific values of the specimens tested, but to find an experimental test that allows studying the evolution of fracture under Mode II conditions, not only inducing a shear stress state at the onset of fracture. After a literature review on shear fracture tests used mainly with concrete, two tests have been selected, a standardised test described by a Japanese standard, here referred to as the JSCE test, and an experimental test that has been recently successfully used to study Mode II fracture in polyolefin-fibre reinforced concrete specimens, the push-off test. These tests have been carried out on fibre-reinforced gypsum specimens with increasing proportions of polypropylene fibres and monitored by means of digital image correlation (DIC). The results show that polypropylene fibres clearly increase the shear behaviour of gypsum, as expected, fibre-reinforced gypsum specimens have a more ductile behaviour than plain gypsum specimens and notably increase their fracture energy before collapsing. Fracture under Mode II conditions is relatively easy to induce with both tests, but once fracture begins, it is extremely difficult to induce a fracture process under Mode II. When the JSCE test is carried out, the onset of fracture is induced under a high shear stress state but then, fracture develops under a combination of Mode I and Mode II, with a decreasing role of the latter. When the push-off test is employed, the experimental work must be very carefully carried out to obtain a true development of fracture under Mode II conditions. Nevertheless, in many cases, fracture begins under a high shear stress state but once it begins, crack progresses under mainly Mode I, only in one case with a high proportion of fibres, fracture has developed under Mode II conditions.

Keywords

Mode II, Shear, Push-off test, Digital Image Correlation, Fibre-reinforced gypsum.

Study of mode II fracture on fibre-reinforced gypsum notched specimens

Fernando Suárez^{a,*}, Javier F. Aceituno^a, Jesús Donaire-Ávila^a

^a*Departamento de Ingeniería Mecánica y Minera. Universidad de Jaén. Campus Científico-Tecnológico de Linares. Cinturón Sur 23700 – Linares (Jaén), Spain*

Abstract

In this paper, two experimental tests used for studying shear fracture in quasibrittle materials are analysed by testing fibre-reinforced gypsum specimens. The main aim of this work is not to measure specific values of the specimens tested, but to find an experimental test that allows studying the evolution of fracture under Mode II conditions, not only inducing a shear stress state at the onset of fracture. After a literature review on shear fracture tests used mainly with concrete, two tests have been selected, a standardised test described by a Japanese standard, here referred to as the JSCE test, and an experimental test that has been recently successfully used to study Mode II fracture in polyolefin-fibre reinforced concrete specimens, the push-off test. These tests have been carried out on fibre-reinforced gypsum specimens with increasing proportions of polypropylene fibres and monitored by means of digital image correlation (DIC). The results show that polypropylene fibres clearly increase the shear behaviour of gypsum, as expected, fibre-reinforced gypsum specimens have a more ductile behaviour than plain gypsum specimens and notably increase their fracture energy before collapsing. Fracture under Mode II conditions is relatively easy to induce with both tests, but once fracture begins, it is extremely difficult to induce a fracture process under Mode II. When the JSCE test is carried out, the onset of fracture is induced under a high shear stress state but then, fracture develops under a combination of Mode I and Mode II, with a decreasing role of the latter. When the push-off test is employed, the experimental work must be very carefully carried out to obtain a true development of fracture under Mode II conditions. Nevertheless, in many cases, fracture begins under a high shear stress state but once it begins, crack progresses under mainly Mode I, only in one case with a high proportion of fibres, fracture has developed under Mode II conditions.

Keywords: Mode II, Shear, Push-off test, Digital Image Correlation, Fibre-reinforced gypsum.

1. Introduction

This study is focused on better understanding Mode II fracture in fibre-reinforced quasibrittle materials, more specifically, fibre-reinforced gypsum. In this section, the importance of fibre reinforcement in construction materials is briefly discussed, then, in order to explain the motivation of this study, a short literature review on Mode II fracture in quasibrittle materials is presented.

1.1. Fibre reinforcement of quasibrittle materials

The use of fibres as reinforcement in construction materials has attracted the interest of many researchers and practitioners in recent years. Concrete is probably the most developed material in this sense, given that the national and international standards [1–3] already provide guidelines for their use as structural reinforcement, which has boosted their usage in recent projects. The benefits of the addition of fibres in quasibrittle matrices are well known and, in the construction field, fibre-reinforced concrete (FRC) is used as provisional interior lining of tunnels during their construction process, as well as in precast concrete elements that are exposed to tension stresses when they are stored or transported to the work site.

*Corresponding author

Email addresses: fsuarez@ujaen.es (Fernando Suárez), jaceitun@ujaen.es (Javier F. Aceituno), jdonaire@ujaen.es (Jesús Donaire-Ávila)

14 In recent years new polymer fibres have started to be used as structural reinforcement of concrete, provid-
15 ing good strengthening properties and not suffering from important disadvantages of traditional steel fibres,
16 such as corrosion, which can be of paramount importance in certain architectural applications, or electric
17 transmissivity, which may limit their use in certain precast elements, such as railway sleepers. Some polymer
18 fibres have proved to be a promising alternative to steel fibres, providing good mechanical properties to FRC
19 under tensile stresses and in different manufacturing conditions [4–6], which has motivated their use in some
20 initial applications as structural reinforcement [7, 8]. The main mechanisms that lead to their good reinforc-
21 ing performance are already identified, with the fibre length and the mechanical properties of the polymeric
22 material being the most relevant.

23 Although concrete attracts most research efforts regarding fibre reinforced construction materials, gypsum
24 can also benefit from this technology. Gypsum is the most widely used material as interior lining in buildings
25 due to, among other reasons, its low cost, easy manipulation, its versatility with different finishes and formats
26 and its hygroscopic and good aesthetic properties. The industry of gypsum has evolved through time, finding
27 new applications and products, such as gypsum plasterboard, which has allowed using this material in a wider
28 range of applications of the construction industry. Nevertheless, not big advances can be observed over the
29 past two decades, and the use of fibres could help extend the use of this material.

30 There are studies about the mechanical properties of fibre-reinforced gypsum (FRG), such as those by
31 García-Santos [9, 10], that analyse how the mechanical properties of gypsum are enhanced with different
32 polymeric fibres. Those studies are old (more than 30 years now) and do not include information about
33 material fracture properties. An interest in using natural fibres, such as flax and hemp, can be observed
34 in recent works, which produces mixes with better mechanical properties and better thermal and acoustic
35 isolation conditions, representing environmentally friendly solutions [11–13]. Some other studies analyse the
36 use of polymer fibres as gypsum reinforcement [14, 15] or the influence of graphite filler additions [16], which
37 not only affect the mechanical properties of the mix, but also its thermal isolation properties.

38 In general, when FRG properties are studied, mechanical tests are usually limited to studying compressive
39 strength, elastic modulus and flexural strength. Nevertheless, fracture energy absorbed by the material before
40 failure can be of great importance in some fields, such as seismic and impact events or differential settlements
41 in structures. In such situations, knowing and modifying the energy that a certain material can absorb before
42 their eventual failure is of great importance in order to design strategies that may increase safety, reduce
43 economic losses or even mitigate the social alarm that the appearance of cracks in building partitions may
44 cause. In this sense, fracture energy is one of the material properties that are notably enhanced with the
45 addition of fibres in gypsum [15].

46 1.2. Mode II fracture in quasibrittle materials

47 Fracture of quasibrittle materials has attracted the attention of many researchers over the last decades,
48 which has allowed understanding the mechanisms involved. When dealing with fracture, three modes are
49 identified, with Mode I corresponding to crack opening perpendicular to the crack direction and being related
50 fundamentally to normal stresses along the crack propagation, Mode II corresponding to a crack lips displace-
51 ment in parallel to the crack direction and being related mainly to shear stresses, and Mode III corresponding
52 to a crack lips displacement out of the plane of the fractured element.

53 There exist many studies and references dealing with Mode I, probably because it is the most usual
54 fracture mechanism in this type of materials. These studies have helped to design reliable experimental tests
55 that measure the parameters that drive this phenomenon, such as the three point bending test [17]. From the
56 numerical side, many fracture models have been proposed over the last decades to reproduce fracture, such as
57 those based on the cohesive zone model [18–21], which can reproduce fracture with remarkable simplicity and
58 accuracy. Some of these models have been adapted in recent years to reproduce fracture of fibre-reinforced
59 quasibrittle materials [22, 23] with numerical methods such as the finite element analysis.

60 Nevertheless, in some occasions fracture results from a combination of modes I and II. In this regard, mode
61 II fracture has been studied less often and not many examples can be found in the literature, partly because
62 mode I fracture is more usual and partly because it is harder to experimentally induce fracture under mode II
63 conditions. From the experimental point of view, some studies have proposed tests to analyse shear fracture,
64 such as the experiment proposed by Nooru-Mohamed [24, 25], which allows combining Mode I and Mode II
65 conditions. Other experimental tests aiming to study shear fracture in concrete are described in [26], two
66 specifically: a test described in the Japanese standard JSCE-G 553-1999 [27] and the push-off test, that has

67 been lately used with success for analysing shear fracture in fibre-reinforced-concrete [28–30]. From the point
 68 of view of numerically reproducing fracture, some models include the effect of the combination of Modes I
 69 and II, like [31–33]. These models need parameters to define the fracture behaviour under Mode I and under
 70 Mode II. While parameters driving Mode I fracture (mainly tensile strength f_t and fracture energy G_F) can be
 71 obtained experimentally with standardised tests [17, 34], parameters related to Mode II are usually estimated,
 72 since their experimental measurement is not easy to obtain.

73 This work aims to deepen the knowledge of the mechanisms involved in fracture of a specimen subjected to
 74 pure shear stresses. To do this, FRG specimens are used and their performance is compared with that of plain
 75 gypsum specimens. FRG specimens are reinforced with polypropylene fibres, usually employed in concrete to
 76 prevent cracking due to shrinkage, and three fibre proportions are analysed: 5, 10 and 20 kg/m³. To induce
 77 shear stresses, two tests are employed, one of them corresponding to an standardised test described in the
 78 Japanese norm [27], that will be here referred to as JSCE test, and the push-off test, that has been lately used
 79 to successfully analyse shear fracture in polyolefinfibre-reinforced concrete (PFRC) [29, 30].

80 2. Description of the study

81 As mentioned above, three FRG mixes have been analysed and compared with a plain gypsum mix, thus,
 82 four mixes have been prepared and their composition can be consulted in Table 1. Plain gypsum reference
 83 mix is identified as 0 and the rest of mixes are identified as A followed by 5, 10 or 20, depending on the fibre
 84 proportion used. In all cases, a water/gypsum ratio of 0.63 is used; this value was obtained following the
 85 procedure described in the UNE-EN 13279-2 standard [35], which determines the mass of gypsum that can be
 86 saturated when it is sprinkled into 100 g of water.

87 The specimens were manufactured following a slight variation of the procedure described in UNE-EN
 88 13279-2 for adding the fibres. Such procedure is described below:

- 89 1. Gypsum was poured on the water and manually mixed for 40 seconds.
- 90 2. Fibres were added and mixed manually for 20 seconds.
- 91 3. Mixing continued for 60 more seconds in a planetary mixer at low speed.
- 92 4. Moulds, previously impregnated with release agent, were filled.
- 93 5. Moulds were hit to eliminate air bubbles and finally levelled.
- 94 6. The specimens were unmoulded and cured inside a controlled-climate chamber for seven days at $23\pm 2^\circ\text{C}$
 95 and relative humidity of $50\pm 5\%$.
- 96 7. Specimens were dried inside an oven at 50°C for 48 hours.
- 97 8. Specimens were cooled at room temperature and the notch was cut with a band saw by dry way.
- 98 9. Specimens were marked with black spray for the later use of digital image correlation (DIC).

Table 1: Composition of the four mixes used in this study

Mix	w/g	Fibres proportion (kg/m ³)
<i>0</i>	0.63	0
<i>A5</i>	0.63	5
<i>A10</i>	0.63	10
<i>A20</i>	0.63	20

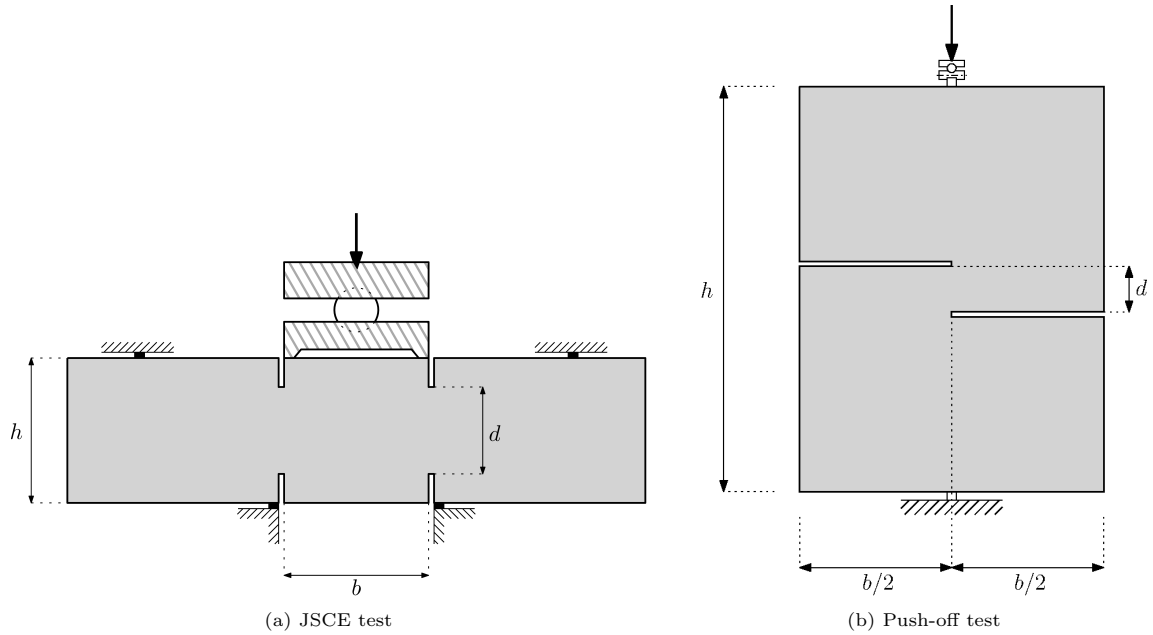


Figure 1: Schemes of the tests used in this work.

99 2.1. JSCE test

100 Figure 1a shows the scheme of this test. A prismatic specimen is doubly notched in two cross sections and
 101 is supported on two points in its lower side and load is applied on two points in the upper side, thus inducing
 102 shear stresses in the vertical ligaments defined by the four notches. External supports placed on the upper
 103 side of the specimen ensure absence of bending during the load application.

104 2.2. Push-off test

105 Figure 1b schematically shows the configuration of this test. A Z-shaped specimen is used and a uniaxial
 106 compression is applied by means of point load in the upper side and a point support in the lower side. The
 107 vertical ligament of length d is then subjected to high shear stresses. This test, as the work by Picazo et
 108 al. shows [29, 30], is very sensitive to small load misalignments, thus a very precise preparation of the test
 109 is necessary. Furthermore, the upper support where load is applied must ensure that no additional torque is
 110 applied, so ball joints or similar solutions must be employed; here a double cylinder joint has been used.

111 3. Materials and methods

112 3.1. Materials

113 Gypsum used in this work is plaster, classified as A1, according to the EN 13279-1 standard [36]. It
 114 is a fine-grained high quality gypsum with a purity over 90%, composed by hemihydrate calcium sulphate
 115 ($\text{CaSO}_4 \cdot 0.5 \text{H}_2\text{O}$) and is commonly used for manufacturing precast elements, such as plasterboard panels used
 116 in sandwich-type partitions.

117 The fibres used here are polypropylene microfibres, named Sikafiber M-12, that are usually employed in
 118 concrete and mortars for reducing their cracking and increasing their durability. They are 12 mm long and
 119 their diameter is 31 μm ; the aspect of these fibres can be observed in Fig. 2.

120 These materials were combined with water to produce the mixes described in Table 1. To produce the
 121 plain gypsum mix, the procedure described in the EN 13279-2 standard [35] was used and, to produce FRG
 122 mixes, a slight variation of it already employed in previous works [15, 37], which includes the addition of fibres
 123 in the last 20 seconds of the manual mixing.



Figure 2: Polypropylene fibres used as reinforcement in the FRG specimens.

124 3.2. Specimens

125 3.2.1. JSCE test specimens

126 Prismatic specimens of 160 mm x 40 mm x 40 mm were manufactured and four notches produced by means
 127 of a band saw. The resulting geometry, according to parameters shown in Fig. 1a corresponds to $h = 40$ mm,
 128 $b = 40$ mm and $d = 24$ mm.

129 3.2.2. Push-off test specimens

130 For this test, 40 mm thick specimens were manufactured and two notches produced with a band saw,
 131 resulting in specimens with the shape shown in Fig. 1b. Notches were extremely carefully produced in order
 132 to ensure good alignment with load and avoid unwanted torsion effects. For this test, two types of specimens
 133 were manufactured, which will be described later; their dimensions, according to parameters of Fig. 1b are
 134 shown in Table 2. The reason that motivated manufacturing of different types of specimens include strategies
 135 for improving the experimental results that will be explained further in Section 4.2.

136 3.3. Experimental setups and methodology

137 In this section the experimental setups employed in both types of tests are described. All tests were
 138 carried out with a dual column testing system of Instron of the 5960 series and using a load cell of 30 kN of
 139 capacity. All tests were analysed with digital image correlation (DIC) by using a Mako U-130B video camera
 140 with a resolution of 1280 x 1024 pixels, and the software Vic-2D, by Correlated Solutions [38]. Digital image
 141 correlation in 2D was performed by employing a 21 pixels size facet and 5 pixels of step.

142 3.3.1. JSCE test

143 Specific steel fixtures were manufactured for this test so that the supports disposition shown in Fig. 1 could
 144 be reproduced. Figure 3 shows the final experimental setup. To ensure applying a centered load and avoid
 145 possible unwanted torques induced by a lack of parallelism between the support lines at the bottoms and those
 146 at the upper side, load was transmitted through a ball joint.

147 Load was applied with a displacement control of 0.25 mm/min up to a maximum displacement of 3 mm
 148 and images for DIC were captured every 5 seconds.

149 3.3.2. Push-off test

150 This test was carried out with two different geometries and specimens were prepared differently in each
 151 case. Each geometry will be referred to as Type 0 and Type 1 hereafter. Figure 4a shows each of these
 152 geometries and Table 2 their dimensions according to parameters defined in Fig. 1.

153 As Picazo et al. report in [29], this test tends to generate flexural stresses at the internal sides of the
 154 notches, to avoid this, some regions of the specimen must be reinforced. Figure 5 shows the S11 and S12

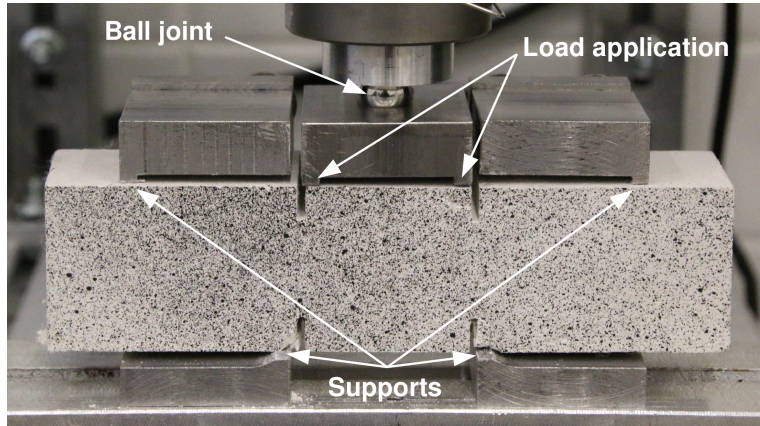


Figure 3: Setup of the JSCE test.

Table 2: Dimensions of push-off specimens according to parameters of Fig. 1b

	h	b	d
	(mm)	(mm)	(mm)
Type 0	160	128	10
Type 1	85	64	14

155 stress fields, which corresponds to σ_x and τ_{xy} components of the stress tensor, respectively, obtained with a
 156 finite element model that reproduces the push-off test for an elastic specimen of the same geometry as Type 0
 157 specimens shown in Figure 4. There is a high concentration of shear stresses along the vertical ligament where
 158 shear fracture is expected, but high tensile stresses can be observed in the horizontal notches due to flexural
 159 strains in the upper and lower cantilevers of the specimen.

160 Type 0 specimens are larger, have thin notches of around 4 mm and were tested using an external steel
 161 reinforcement fixed by means of hand clamps, as can be observed in Figure 4b. This disposition had some
 162 benefits, like easier preparation and a larger visible area in the region of interest defined by both notches,
 163 where Mode II fracture is expected. Nevertheless, it also had some disadvantages, as will be discussed later.

164 Type 1 specimens are smaller, have thicker notches of around 15 mm and were reinforced with external
 165 glass fibre reinforcement fixed with polyester resin. The purpose of this external reinforcement is avoiding
 166 unwanted Mode I fracture due to flexural stresses (see Figure. 5). Thicker notches allowed reinforcing internal
 167 sides of notches and some additional benefits, although they also presented some disadvantages, as it will be
 168 observed later.

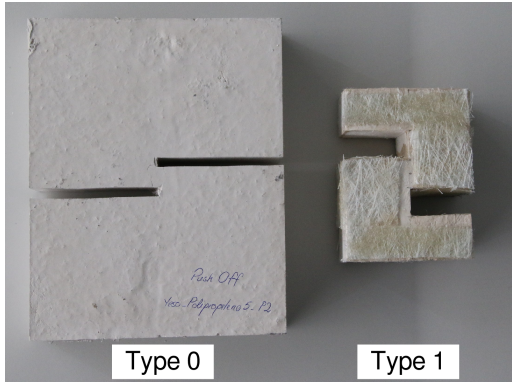
169 4. Results

170 In this section, the experimental results are presented. Firstly, the results obtained with the JSCE test will
 171 be shown and later the results corresponding to both specimen types of the push-off tests will be presented.

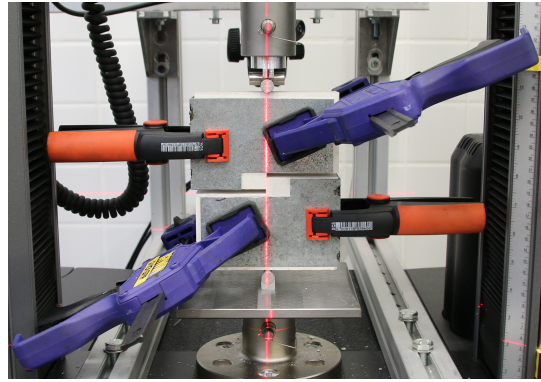
172 4.1. JSCE test

173 Figure 6 shows the load-displacement diagrams of all the tested specimens. Plain gypsum specimens are
 174 represented in grey and A5, A10 and A20 FRG mixes are represented in blue, green and red, respectively.
 175 Line formats allow identification of different specimens of the same mix.

176 Fibre reinforcement results in higher strength and, although some general trends can be identified, no clear
 177 differences between increasing fibre proportions can be observed, especially between mixes A5 and A10. In all



(a) Type 0 and Type 1 specimens of the push-off test.



(b) General view of the setup with a Type 0 specimen.

Figure 4: (a) Type 0 and Type 1 specimens of the push-off test; (b) Experimental setup of the push-off test.

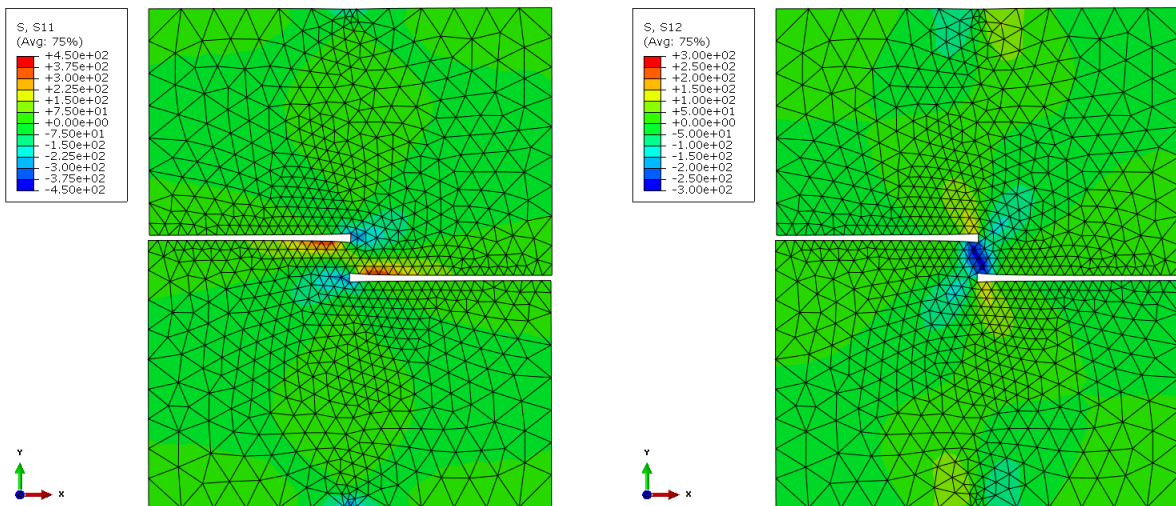


Figure 5: S11 (σ_x) and S12 (τ_{xy}) fields obtained with an elastic finite element model of the push-off test.

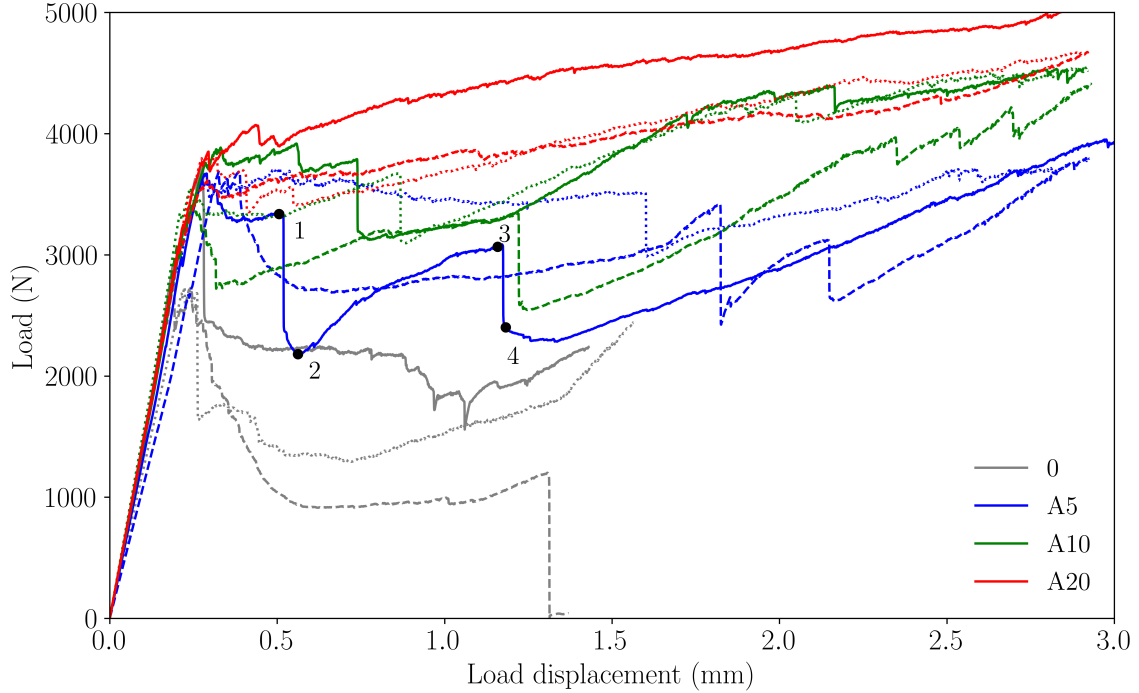


Figure 6: Load displacement diagrams obtained with the JSCE test. Mixes are identified with different colours.

FRG mixes, the peak load is higher when compared with plain gypsum specimens; nevertheless, interpreting these results is not trivial. In all FRG specimens several load drops and load increments are observed along the test, although these are more evident in A5 and A10 specimens, since A20 specimens present an almost constant load increment after an initial elastic behaviour. Finally, it is interesting to note that material ductility is greatly enhanced by fibre addition, ductility increases with fibre proportion, but is also relevant even with small proportions of fibres.

If A5 specimen represented with a solid line in Figure 6 is observed, all the main failure mechanisms that take place during the test can be identified:

- Load initially increases linearly with the displacement, which corresponds to an elastic behaviour before any damage develops in the specimen.
- Just after the linear behaviour ends, an almost horizontal plateau is observed, which is related to local damage around some supports.
- The first load drop (between points 1 and 2) identifies the first crack at one of the notches. Once it is produced, load increases again due to the fibre reinforcement (between points 2 and 3), which strengthens the cracked region.
- The second load drop (between points 3 and 4) identifies the appearance of a second crack, after which, again, fibre reinforcement allows a new load increment.

Figure 7 shows the ε_x and ε_{xy} strain fields obtained with the digital image correlation technique for this specimen (first specimen of A5 mix) at four representative instants of the load-displacement diagram, that are identified by numbers 1 to 4 in Figure 6:

- Point 1: This point identifies the instant just before the first load drop is observed. The DIC images show that, apart from local damage around the supports and the load application points, shear strain (ε_{xy}) concentrates along both vertical planes defined by notches. Note that the extreme values of the colour scale identify the same shear strain, although of different sign, which implies that both vertical

202 planes are subjected to similar shear strains. On another note, ε_x strains suggest that the portion of the
 203 specimen between both vertical shear planes is subjected to bending, since the ε_x strain field presents
 204 compression strains at the upper half and tension strains at the lower half.

- 205 • Point 2: These results correspond to the first frame after the first load drop. The DIC images show
 206 clearly the initiation of the first crack, which occurs at the bottom notch of the right plane. The ε_x
 207 strain field shows a very high concentration of these strains along the crack, which, since the crack is
 208 mainly vertical, evidences a crack opening where Mode I plays an important role together with Mode II.
- 209 • Point 3: Just before the second load drop, the DIC images show that the first crack has evolved under a
 210 combination of Mode I and Mode II, with the former being the predominant mode. In the left vertical
 211 shear plane, there is again a high concentration of shear strains.
- 212 • Point 4: These results show the strain fields just after the second load drop. A new crack appears at the
 213 left vertical shear plane, which is responsible for this second load drop.

214 In this test, several issues make interpretation of the experimental results difficult. First of all, each
 215 specimen has two possible fracture planes, which makes it hard to measure material fracture properties.
 216 Secondly, in the case of FRG, local damage develops around the supports, which affects the resulting load-
 217 displacement diagram. Thirdly, fracture develops in several places along the test, up to four possible cracks.
 218 Finally, if the displacement is large enough, the central region of the specimen usually rotates, which modifies
 219 the way load is transmitted in the specimen; for example, when this rotation is large enough, the central portion
 220 of the specimen contacts the lateral portions, therefore, the load is not only transmitted along the vertical
 221 planes defined by the notches, but also through these contacts, thus resulting in a complex load transmission
 222 that no longer permits the study of Mode II fracture.

223 In addition to the previous issues, the way cracking develops in each of the cracks produced during the test
 224 suggest that fracture is due to a combination of Modes I and II, since crack lips do not move in parallel to
 225 each other, but an evident crack opening in perpendicular to them is clearly observed. Therefore, even if all
 226 the issues mentioned above could be avoided, the resulting fracture process would not serve to measure Mode
 227 II fracture, since Mode I would also be involved.

228 4.2. Push-off test

229 Figure 8 shows the shear stress-displacement diagrams obtained with the Type 0 specimens. The value of
 230 the shear stress τ is obtained as load divided by the area of the ligament subjected to shear:

$$\tau = \frac{P}{d \cdot t} \quad (1)$$

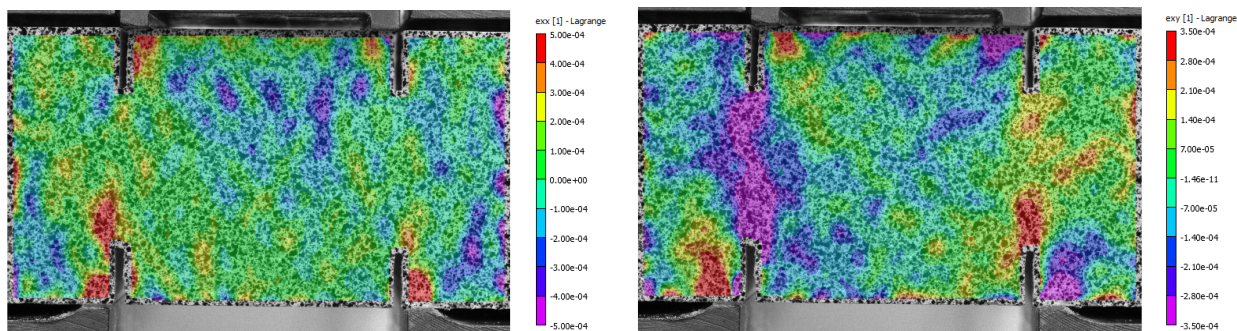
231 where P refers to the load, d represents the ligament length (see Figure 1) and t the specimen thickness, which
 232 in this case equals 40 mm.

233 As in Figure 8, each colour identifies each mix, with the grey colour identifying the plain gypsum specimens
 234 and blue, green and red identifying A5, A10 and A20 mixes. Three specimens of each mix have been tested,
 235 each specimen of a mix has a different line format to allow easy identification.

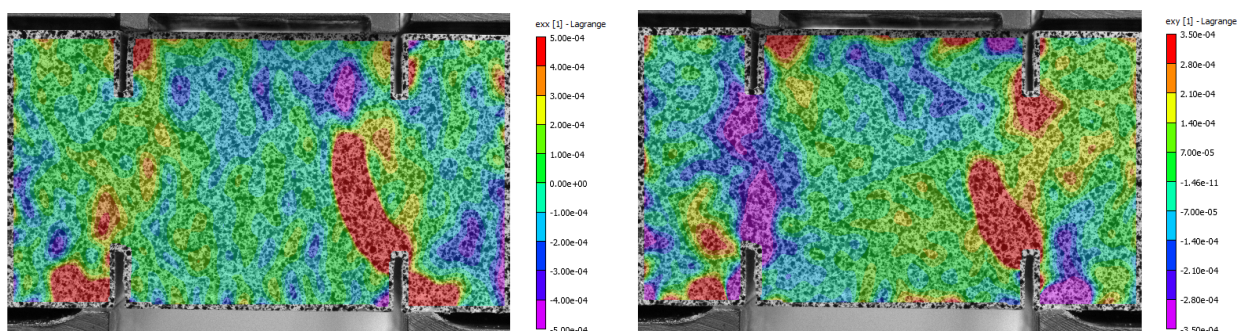
236 These results show an important experimental scatter, usual in this type of material. The most remarkable
 237 effect of fibre reinforcement can be observed in how the load drop after the peak load becomes smaller as the
 238 fibre proportion increases.

239 Apart from the load-displacement diagrams, when the digital image correlation results are analysed, if the
 240 horizontal direction is identified as the x axis and the vertical direction as the y axis, before fracture takes
 241 place, shear strain ε_{xy} is high along the vertical ligament where Mode II fracture is expected but, once fracture
 242 occurs, two unwanted issues are identified:

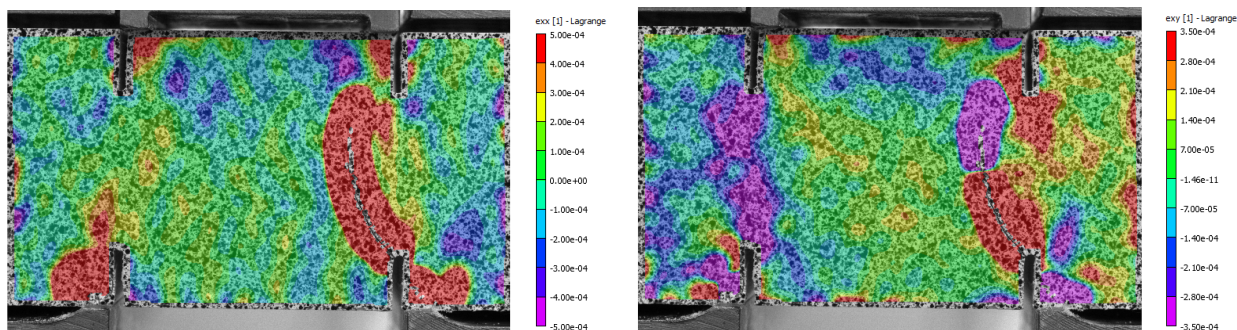
- 243 • Fracture often occurs outside the vertical ligament where shear fracture is expected.
- 244 • Crack develops with crack lips moving apart from each other, not in parallel, thus revealing a Mode I
 245 fracture, rather than a fracture evolution in Mode II.



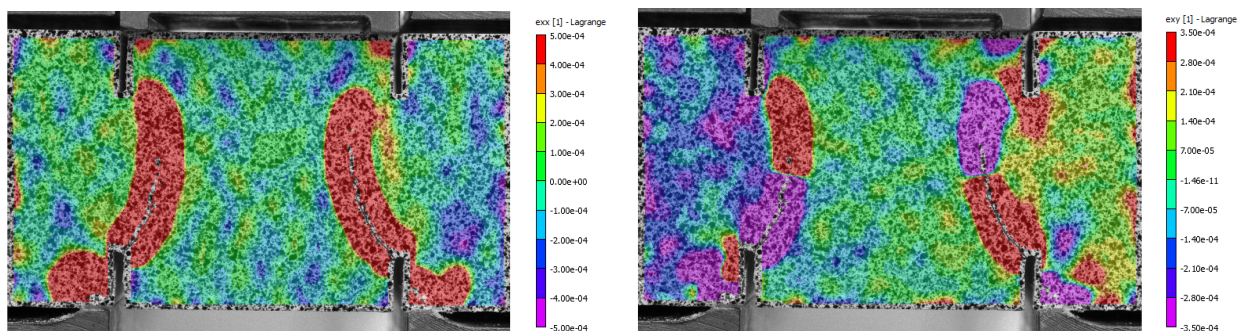
(a) Point 1 in Figure 6: (left): ε_x , (right): ε_{xy} .



(b) Point 2 in Figure 6: (left): ε_x , (right): ε_{xy} .



(c) Point 3 in Figure 6: (left): ε_x , (right): ε_{xy} .



(d) Point 4 in Figure 6: (left): ε_x , (right): ε_{xy} .

Figure 7: Strains field ε_x (left) and ε_{xy} (right) of specimen 1 of A5 mix at four instants during the JSCE test, identified by points 1 to 4 shown in Figure 6.

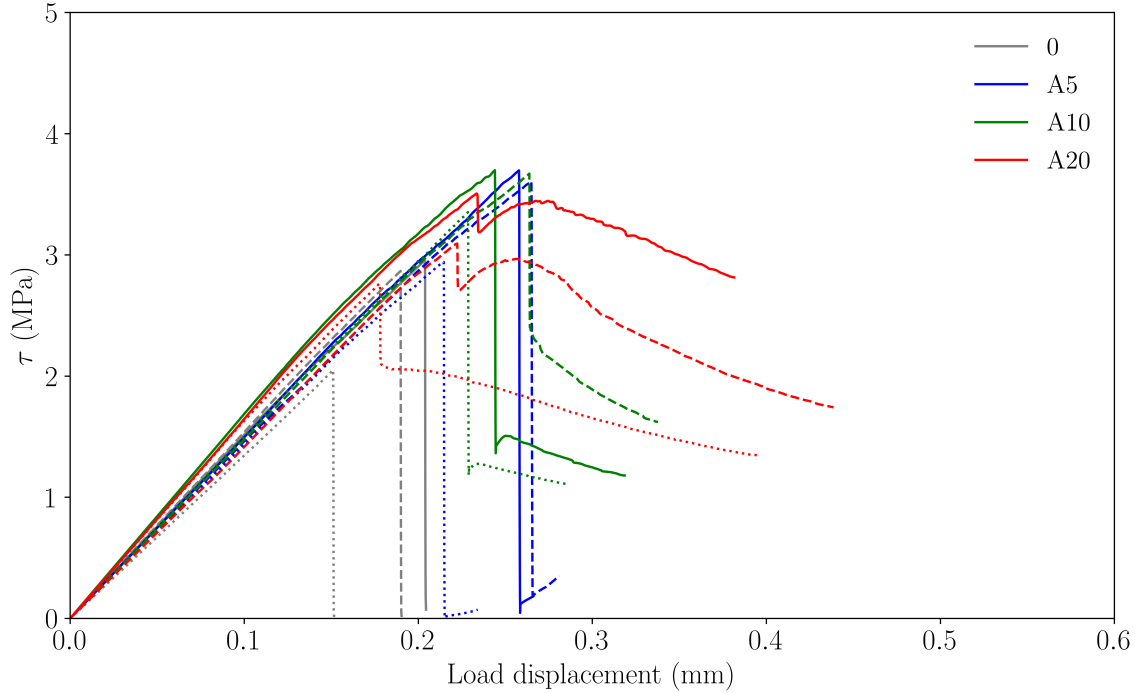


Figure 8: Load displacement diagrams obtained with the push-off test using Type 0 specimens (see Figure 4a). Mixes are identified with different colours.

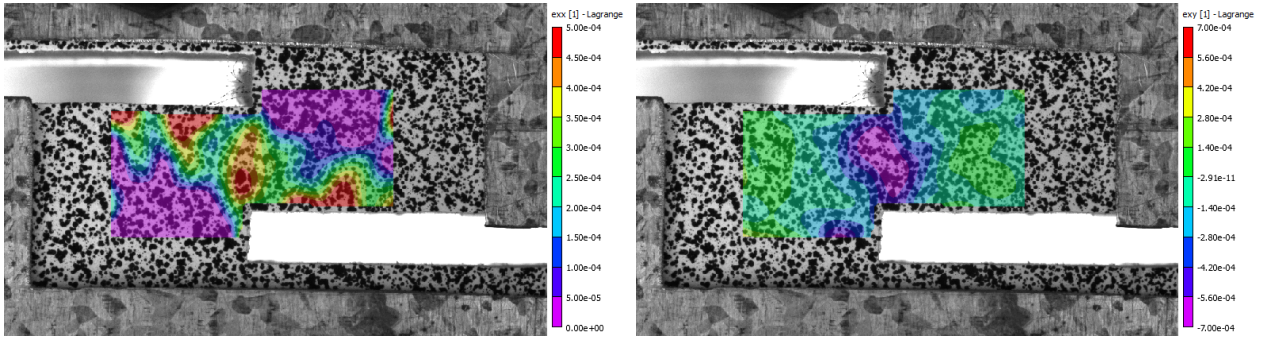
246 Figure 9a) shows the ε_x and ε_{xy} strain fields just before the onset of fracture, revealing that shear strain
 247 is high along the vertical shear ligament, although horizontal strains appear along the horizontal notches.
 248 Therefore, three fracture mechanisms are in competition: the shear failure along the vertical ligament and the
 249 tensile failure on both horizontal notches.

250 Finally, as shown in Figure 9b), failure develops in one of the horizontal notches, which means that failure
 251 does not occur due to shearing but due to indirect tensile stresses induced by bending of the cantilevers. As
 252 Figure 9b) also shows, the crack develops mainly under Mode I conditions, since the crack lips fundamentally
 253 move apart from each other in perpendicular to the crack path.

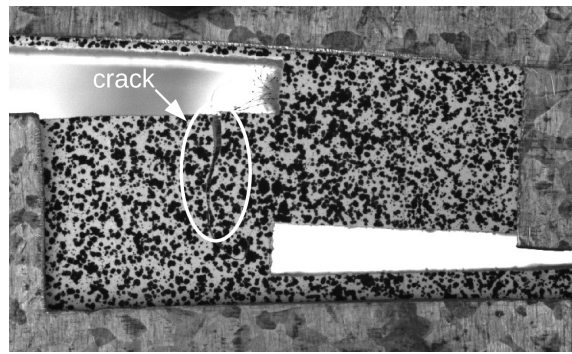
254 These results suggest that, although the specimen is subjected to shear loading and, in fact, a high concen-
 255 tration of shear stresses is reached along the vertical ligament before the onset of fracture, fracture eventually
 256 takes place in another region and develops as Mode I fracture. Therefore, these results are not providing
 257 information about Mode II fracture development. On another note, as fracture develops, both halves of the
 258 specimen rotate around the crack until two lips of a notch contact each other, then providing no longer valid
 259 results of the test.

260 These issues are the reason why a new set of specimens are tested using the Type 1 geometry shown in
 261 Figure 4a. This geometry allows reinforcing the sides of the notches where flexural stresses lead to unwanted
 262 Mode I fracture and permits carrying out the test up to larger load displacement values, providing more
 263 complete test results.

264 Figure 10 shows the shear stress-displacement diagrams obtained with the Type 1 specimens, which were
 265 carried out only with FRG mixes. These diagrams show a remarkably different behaviour between mixes, with
 266 a general trend showing that increasing proportions of fibres leads to higher ductilities, as observed in the case
 267 of the JSCE test, but some results are, in principle, unexpected. In all mixes, very different behaviours can
 268 be observed between each pair of specimens and, apparently, specimens of different mixes have a very similar
 269 behaviour between each other, but very different with respect to the other specimen of the same mix. For
 270 example, results marked with I in the figure correspond to different mixes but have a quite similar post-peak
 271 behaviour, which is the part of the diagram more influenced by the fibre addition. Likewise, results marked
 272 with II also correspond to different mixes and also have a very similar behaviour if compared with each other,



(a) Strains field of one specimen of A5 mix just before fracture occurs; (left): ε_x , (right): ε_{xy} .



(b) Image of the specimen once fracture has developed.

Figure 9: Strains fields of one specimen of A5 mix just before fracture occurs and b) image of the specimen once fracture has developed. The circle shows that crack has not developed along the shear plane.

273 being different to the other specimens of the same mixes. This can be explained by observing the images
 274 obtained during the tests. Figure 11 shows two images that help to understand these differences and why
 275 some results cannot be considered as valid:

- 276 • Results identified with I in Figure 10 correspond to the case shown in Figure 11a, where fracture does
 277 not develop along the vertical shear plane, but inside the reinforced region, that is why fracture cannot
 278 be observed in this image, since it is hidden by the glass fibre reinforcement.
- 279 • Results identified with II in Figure 10 fails as shown in Figure 11b. These specimens do fail along
 280 the vertical shear plane, as expected, but crack does not develop under mode II conditions. Once crack
 281 opens, fracture develops under Mode I conditions, since the upper half and the lower half of the specimen
 282 rotate around each other, thus crack lips separate from each other perpendicularly to the crack path.

283 Regarding the result identified with III in Figure 10, the test is clearly invalid since fracture does not take
 284 place along the vertical shear ligament, but in the lower cantilever where the lower support is applied.

285 Finally, the result identified with IV in Figure 10 corresponds to a specimen in which fracture does take
 286 place along the vertical shear ligament and develops as shown in Figure 12. These results show the evolution
 287 of three fields: ε_x and ε_{xy} strain fields and the vertical displacement field v in this specimen at different
 288 stages of the test, where a) is the instant just before the load drop occurs and results b) and c) are two
 289 subsequent instants. Fracture evolves with high concentration of shear strain ε_{xy} along the vertical ligament
 290 and, differently from other cases like the one shown in Figure 9b), where fracture developed in clear Mode I
 291 conditions, here Mode II is predominant, which can be observed in the evolution of the vertical displacement
 292 field v . Just before fracture, no relative vertical displacement can be observed between the left and right
 293 halves of the specimen, but once fracture starts, both halves clearly move vertically with respect to each other
 294 along the vertical ligament (note the evolution of the v field in Figure 12). Finally, if the evolution of ε_x
 295 is observed, Mode I is also present, although its relevance is less important than in other cases.

296 These results suggest that in this specimen, not only the onset of fracture is strongly influenced by shear
 297 stresses, which also happened in other specimens (see Figure 9), but fracture also evolves strongly due to
 298 shearing, following a similar evolution as expected for Mode II (see Figure 1). Nevertheless, this shearing is
 299 not pure, and tensile stresses, associated with Mode I, is also present, although with a smaller relevance than
 300 in other specimens where fracture mainly occurred under Mode I conditions (see Figs. 9b and 11b).

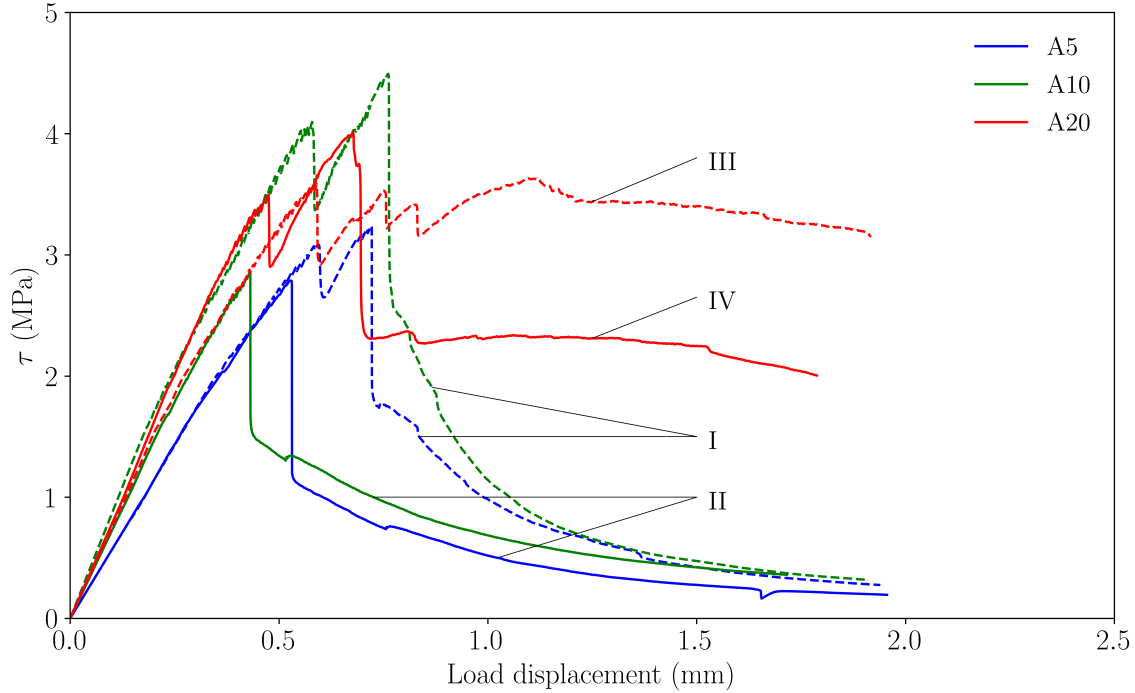


Figure 10: Load displacement diagrams obtained with the push-off test using Type 1 specimens (see Figure 4a). Mixes are identified with different colours.

301 5. Conclusions

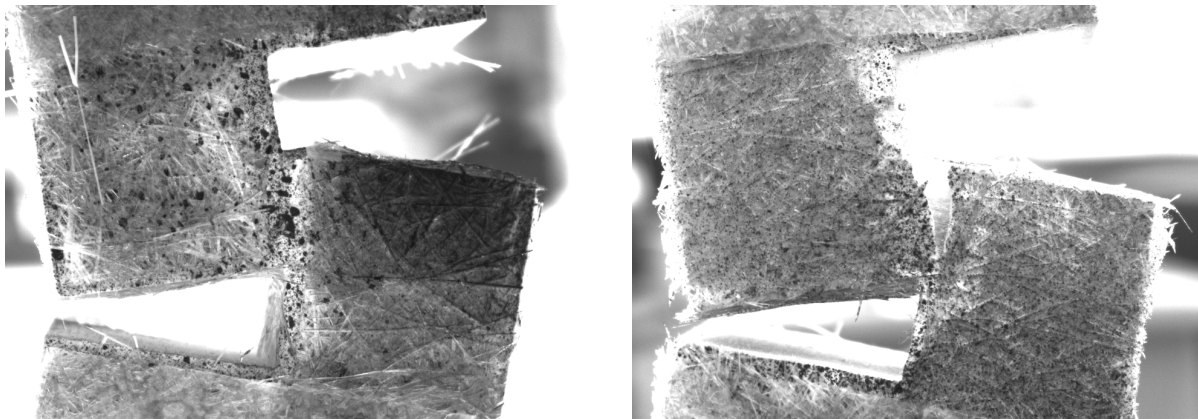
302 5.1. JSCE test

303 The results obtained with the JSCE test show that an increasing proportion of fibres modify the behaviour
 304 of the material, resulting in a slightly higher initial peak load, a higher bearing capacity after it and an overall
 305 increase of ductility. Fibres act as a bonding bridge between both crack lips, thus increasing the bearing
 306 capacity of the specimen.

307 This test requires a quite complex experimental setup and produces results that are not easy to interpret due
 308 to the reasons mentioned in Section 4.1, like the damage around the supports or the shear damage induced in
 309 two planes at the same time. Nevertheless, it effectively induces a strong shear stress state along both vertical
 310 ligaments where fracture is expected, as DIC analysis reveals, but once fracture starts, it does not clearly
 311 evolve under pure Mode II. In fact, DIC analysis suggests that Mode I is predominant in the crack opening
 312 process. Moreover, the crack pattern resembles the results obtained with other tests like those suggested by
 313 Nooru-Mohamed [24, 25] and Bocca [39], leading to a crack opening evolution that combines Mode I and Mode
 314 II, with the former being predominant over the latter, as already observed in [40].

315 5.2. Push-off test

316 The results obtained with the push-off test also show a strengthening effect of the addition of fibres,
 317 especially after the peak load, with an interesting ductility of the material that increases with the fibre
 318 proportion.



(a) One of the specimens marked with I in Figure 10.

(b) One of the specimens marked with II in Figure 10.

Figure 11: Last frames of two push-off tests on Type 1 specimens.

319 In this test, results interpretation is not difficult, since only one fracture shear ligament is loaded and no
 320 damage previous to the peak load is observed. DIC analysis reveals that shear strain is effectively induced
 321 along the vertical ligament, but shear fracture mechanism competes with secondary bending phenomena that
 322 may lead to fracture in a different region of the specimen and lead to a different fracture process, more related
 323 to Mode I rather than Mode II.

324 The specimen geometry and the experimental setup must be carefully designed, since this test is particularly
 325 sensitive to any misalignment of loading, as proves the fact that only one of the specimens has produced a
 326 quite satisfactory result.

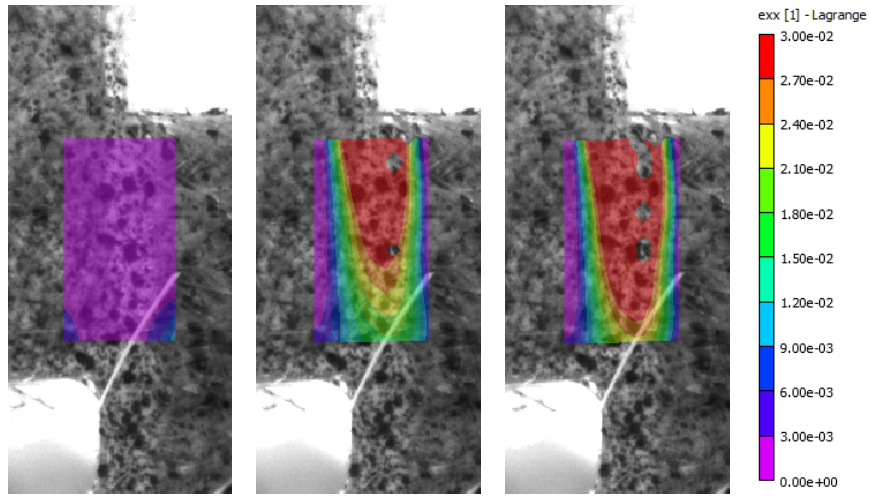
327 Push-off test results show that producing fracture under strong shearing conditions is relatively easy with
 328 this experimental setup, but fracture evolution under Mode II conditions is extremely hard to obtain. Only
 329 one of the more heavily reinforced specimens (A20 mix) has resulted in a fracture evolution quite similar to the
 330 theoretical Mode II, but even in this case, Mode I has also a relevant role, as DIC results prove (see Figure 12).

331 Acknowledgements

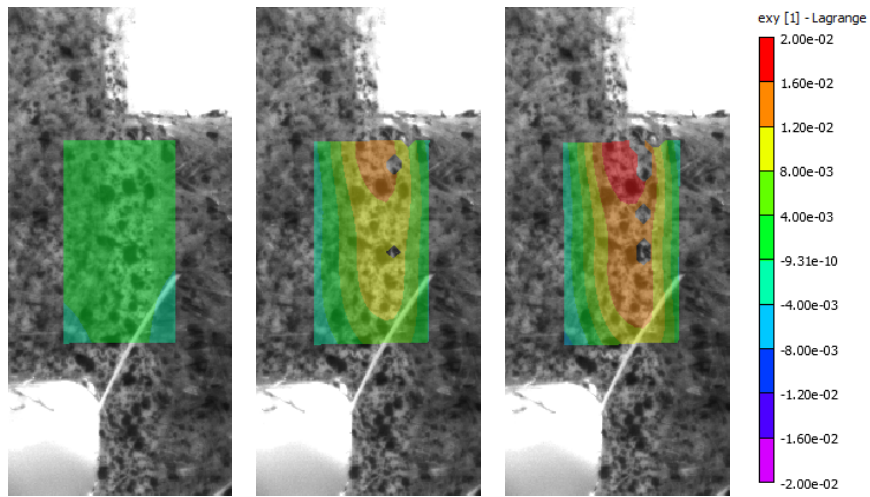
332 Authors gratefully acknowledge the financial support provided by Universidad de Jaén through Action 1
 333 of the Support to transfer of knowledge, entrepreneurship and employability plan of this university, which has
 334 allowed carrying out the experimental tests described in this study.

335 References

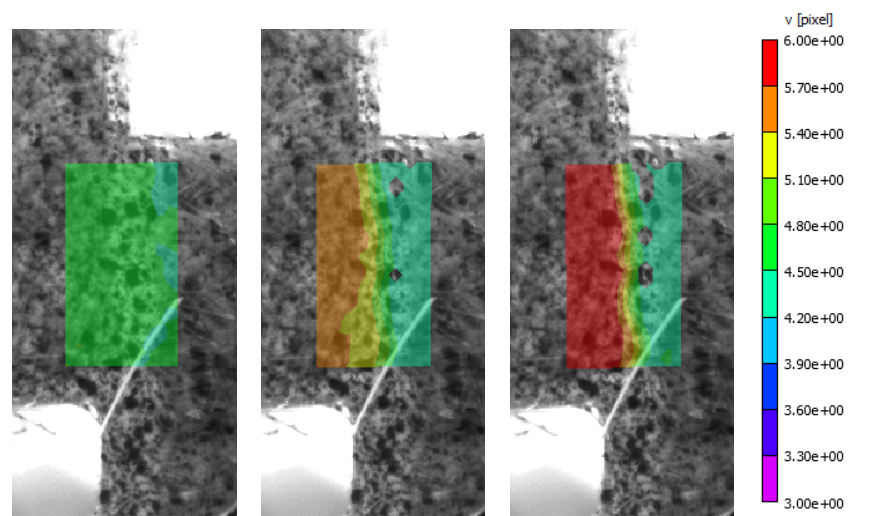
- 336 [1] CNR-DT 204. Guide for the Design and Construction of Fiber-Reinforced Concrete Structures, Consiglio Nazionale delle
 337 Ricerche: Roma, Italy, 2006.
- 338 [2] EHE-08, Instrucción de hormigón estructural, Ministerio de Fomento, Madrid, España, 2008.
- 339 [3] C.-F. M. Code, Fib model code for concrete structures 2010; ernst & sohn, Wiley: Berlin, Germany (2013).
- 340 [4] M. Alberti, A. Enfedaque, J. Gálvez, Comparison between polyolefin fibre reinforced vibrated conventional concrete and
 341 self-compacting concrete, *Construction and Building Materials* 85 (2015) 182–194.
- 342 [5] M. Alberti, A. Enfedaque, J. Gálvez, Fibre reinforced concrete with a combination of polyolefin and steel-hooked fibres,
 343 *Composite Structures* 171 (2017) 317–325.
- 344 [6] M. Alberti, A. Enfedaque, J. Gálvez, Fracture mechanics of polyolefin fibre reinforced concrete: Study of the influence of
 345 the concrete properties, casting procedures, the fibre length and specimen size, *Engineering Fracture Mechanics* 154 (2016)
 346 225–244.
- 347 [7] M. G. Alberti, J. C. Gálvez, A. Enfedaque, A. Carmona, C. Valverde, G. Pardo, Use of steel and polyolefin fibres in the
 348 canda tunnels: Applying mives for assessing sustainability evaluation, *Sustainability* 10 (12) (2018) 4765.
- 349 [8] M. G. Alberti, A. Enfedaque, J. C. Gálvez, L. Pinillos, Structural cast-in-place application of polyolefin fiber-reinforced
 350 concrete in a water pipeline supporting elements, *Journal of Pipeline Systems Engineering and Practice* 8 (4) (2017) 05017002.
- 351 [9] A. García Santos, Comportamiento mecánico de yeso reforzado con polímeros sintéticos, Ph.D. thesis, Arquitectura (1988).
- 352 [10] A. G. Santos, Escayola reforzada con fibras de polipropileno y aligerada con perlas de poliestireno expandido/escayola reforzada
 353 con fibras de polipropileno y aligerada con perlas de poliestireno expandido, *Materiales de Construcción* (293) (2009) 105–124.



(a) ε_x : (left): instant before load drop occurs, (center) and (right): subsequent instants.



(b) ε_{xy} : (left): instant before load drop occurs, (center) and (right): subsequent instants.



(c) v : (left): instant before load drop occurs, (center) and (right): subsequent instants.

Figure 12: Evolution of the ε_x and ε_{xy} strain fields and the vertical displacement field v for the specimen of the A20 mix identified with IV in Figure 10.

- 354 [11] P. Dalmay, A. Smith, T. Chotard, P. Sahay-Turner, V. Gloaguen, P. Krausz, Properties of cellulosic fibre reinforced plaster:
355 influence of hemp or flax fibres on the properties of set gypsum, *Journal of materials science* 45 (3) (2010) 793–803.
- 356 [12] F. Iucolano, B. Liguori, P. Aprea, D. Caputo, Thermo-mechanical behaviour of hemp fibers-reinforced gypsum plasters,
357 *Construction and Building Materials* 185 (2018) 256–263.
- 358 [13] F. Iucolano, L. Boccarusso, A. Langella, Hemp as eco-friendly substitute of glass fibres for gypsum reinforcement: Impact
359 and flexural behaviour, *Composites Part B: Engineering* 175 (2019) 107073.
- 360 [14] C. Zhu, J. Zhang, J. Peng, W. Cao, J. Liu, Physical and mechanical properties of gypsum-based composites reinforced with
361 pva and pp fibers, *Construction and Building Materials* 163 (2018) 695–705.
- 362 [15] F. Suárez, L. Felipe-Sesé, F. Díaz, J. Gálvez, M. Alberti, On the fracture behaviour of fibre-reinforced gypsum using micro
363 and macro polymer fibres, *Construction and Building Materials* 244 (2020) 118347.
- 364 [16] M. del Mar Barbero-Barrera, N. Flores-Medina, V. Pérez-Villar, Assessment of thermal performance of gypsum-based com-
365 posites with revalorized graphite filler, *Construction and Building Materials* 142 (2017) 83–91.
- 366 [17] D. R. RILEM, Determination of the fracture energy of mortar and concrete by means of three-point bend tests on notched
367 beams, *Materials and structures* 18 (106) (1985) 285–290.
- 368 [18] J. C. Simo, J. Oliver, F. Armero, An analysis of strong discontinuities induced by strain-softening in rate-independent
369 inelastic solids, *Computational mechanics* 12 (5) (1993) 277–296.
- 370 [19] Y.-N. Li, Z. P. Bažant, Cohesive crack model with rate-dependent opening and viscoelasticity: Ii. numerical algorithm,
371 behavior and size effect, *International journal of fracture* 86 (3) (1997) 267–288.
- 372 [20] J. M. Sancho, J. Planas, D. A. Cendón, E. Reyes, J. Gálvez, An embedded crack model for finite element analysis of concrete
373 fracture, *Engineering fracture mechanics* 74 (1-2) (2007) 75–86.
- 374 [21] M. Jirásek, Damage and smeared crack models, in: *Numerical modeling of concrete cracking*, Springer, 2011, pp. 1–49.
- 375 [22] M. Alberti, A. Enfedaque, J. Gálvez, E. Reyes, Numerical modelling of the fracture of polyolefin fibre reinforced concrete by
376 using a cohesive fracture approach, *Composites Part B: Engineering* 111 (2017) 200–210.
- 377 [23] P. Havlásek, P. Kabele, A detailed description of the computer implementation of shcc material model in oofem, CTU in
378 Prague (2017).
- 379 [24] M. B. Nooru-Mohamed, Mixed-mode fracture of concrete: An experimental approach., Ph.D. thesis, Delft University of
380 Technology (1992).
- 381 [25] M. Nooru-Mohamed, E. Schlangen, J. G. van Mier, Experimental and numerical study on the behavior of concrete subjected
382 to biaxial tension and shear, *Advanced cement based materials* 1 (1) (1993) 22–37.
- 383 [26] T. Soetens, S. Matthys, Shear-stress transfer across a crack in steel fibre-reinforced concrete, *Cement and Concrete Composites*
384 82 (2017) 1–13.
- 385 [27] JSCE-G 553-1999. Test method for shear strength of steel fiber reinforced concrete, *Standard Specifications for Concrete*
386 *Structures, Test Methods and Specifications*, Japan Society of Civil engineers (JSCE), Tokyo, 2005.
- 387 [28] F. O. Navas, J. Navarro-Gregori, G. L. Herdocia, P. Serna, E. Cuenca, An experimental study on the shear behaviour of
388 reinforced concrete beams with macro-synthetic fibres, *Construction and Building Materials* 169 (2018) 888–899.
- 389 [29] A. Picazo, J. Gálvez, M. Alberti, A. Enfedaque, Assessment of the shear behaviour of polyolefin fibre reinforced concrete and
390 verification by means of digital image correlation, *Construction and Building Materials* 181 (2018) 565–578.
- 391 [30] A. Picazo, M. Alberti, J. Gálvez, A. Enfedaque, Shear slip post-cracking behaviour of polyolefin and steel fibre reinforced
392 concrete, *Construction and Building Materials* 290 (2021) 123187.
- 393 [31] D. Cendón, J. Gálvez, M. Elices, J. Planas, Modelling the fracture of concrete under mixed loading, *International journal of*
394 *fracture* 103 (3) (2000) 293–310.
- 395 [32] V. O. García-Álvarez, R. Gettu, I. Carol, Numerical analysis of mixed mode fracture in concrete using interface elements, in:
396 *Proceedings of the European Congress on Computational Methods in Applied Sciences and Engineering*, Barcelona, Spain,
397 2000, pp. 11–14.
- 398 [33] F. Suárez, J. Gálvez, D. Cendón, A material model to reproduce mixed-mode fracture in concrete, *Fatigue & Fracture of*
399 *Engineering Materials & Structures* 42 (1) (2019) 223–238.
- 400 [34] ASTM, C. 496-96. Standard test method for splitting tensile strength of cylindrical concrete specimens, 1996.
- 401 [35] UNE-EN 13279-2. Gypsum binders and gypsum plasters – Part 2: Test methods, 2014.
- 402 [36] UNE-EN 13279-1. Gypsum binders and gypsum plasters – Part 1: Definitions and requirements, 2009.
- 403 [37] F. Suárez Guerra, L. Felipe-Sesé, F. Díaz, J. Gálvez Ruiz, M. García Alberti, Comportamiento en fractura de yeso con
404 adición de fibras poliméricas, in: *Anales de Mecánica de Fractura*, Vol. 36, Secretaría del Grupo Español de la Fractura,
405 2019, pp. 114–119.
- 406 [38] C. S. Vic-2D, Reference manual (2009).
- 407 [39] P. Bocca, A. Carpinteri, S. Valente, Mixed mode fracture of concrete, *International Journal of Solids and Structures* 27 (9)
408 (1991) 1139–1153.
- 409 [40] J. A. Alonso Vera, Estudio de la fisuración en particiones verticales de yeso laminado, producidas por la deformación de
410 forjados, Ph.D. thesis, E.T.S.I. Caminos, Canales y Puertos, (UPM), Madrid (2015).